JCB Article

Role of KIFC3 motor protein in Golgi positioning and integration

Ying Xu, Sen Takeda, Takao Nakata, Yasuko Noda, Yosuke Tanaka, and Nobutaka Hirokawa

Department of Cell Biology and Anatomy, Graduate School of Medicine, University of Tokyo, 7-3-1 Hongo, Tokyo 113-0033, Japan

KIFC3, a microtubule (MT) minus end–directed kinesin superfamily protein, is expressed abundantly and is associated with the Golgi apparatus in adrenocortical cells. We report here that disruption of the *kifC3* gene induced fragmentation of the Golgi apparatus when cholesterol was depleted. Analysis of the reassembly process of the Golgi apparatus revealed bidirectional movement of the Golgi fragments in both wild-type and *kifC3*$^{-/-}$ cells. However, we observed a markedly reduced inwardly directed motility of the Golgi fragments in cholesterol-depleted *kifC3*$^{-/-}$ cells compared with either cholesterol-depleted wild-type cells or cholesterol-replenished *kifC3*$^{-/-}$ cells. These results suggest that (a) under the cholesterol-depleted condition, reduced inwardly directed motility of the Golgi apparatus results in the observed Golgi scattering phenotype in *kifC3*$^{-/-}$ cells, and (b) cholesterol is necessary for the Golgi fragments to attain sufficient inwardly directed motility by MT minus end–directed motors other than KIFC3, such as dynein, in *kifC3*$^{-/-}$ cells. Furthermore, we showed that Golgi scattering was much more drastic in *kifC3*$^{-/-}$ cells than in wild-type cells to the exogenous dynamitin expression even in the presence of cholesterol. These results collectively demonstrate that KIFC3 plays a complementary role in Golgi positioning and integration with cytoplasmic dynein.

Introduction

Kinesin superfamily proteins (KIFs)* are molecular motors that sort and transport proteins and lipids along microtubules (MTs) (Hirokawa, 1998). Recent studies identified a number of COOH-terminal motor domain type KIF proteins (KIFC2/KIFC3) using a PCR primer corresponding to KIFC consensus sequences (Hanlon et al., 1997; Saito et al., 1997; Noda et al., 2001). Similar to cytoplasmic dynein (CyDy), these proteins were assumed to be MT minus end–directed motors. However, it is still controversial whether KIFCs have roles distinct from those of CyDy or whether they play redundant roles in cooperation with CyDy. In this study, we disrupted the *kifC3* gene that encodes an MT minus end–directed motor protein and found that KIFC3 plays an essential role in Golgi positioning under the cholesterol-depleted condition.

In higher eukaryotic cells, the Golgi apparatus is centralized around the centrosome and has been proposed to be linked to the minus end of MTs by Golgi microtubule-associated protein (GMAP) for its activity (Infante et al., 1999). This is an optimal localization for enabling transport intermediates derived from the ER to use radially arranged MTs to converge at the central localization (Rothman and Wieland, 1996). A major focus of current works in this area has been to clarify the role of molecular motors in regulating the balance of membrane inflow and outflow pathways that underlie Golgi membrane dynamics (Lippincott-Schwartz et al., 1998; Allan and Schroer, 1999; Valderrama et al., 2001). Among them, CyDy has been proposed to play an important role in ER-to-Golgi transport as well as Golgi localization. Blocking this transport by disruption of CyDy induces the scattering of Golgi fragments at or near their ER exit sites (Vaisberg et al., 1996; Burkhardt et al., 1997; Presley et al., 1997; Harada et al., 1998). However, this strategy blocks the early stage of the Golgi structure maintenance, which impedes the observation of the following processes of Golgi integration and positioning. More importantly, it is not known whether Golgi positioning is determined by CyDy only, or by the balance of multiple motors, as in the case of the mitotic apparatus (Stearns, 1997).

On the other hand, recent studies have revealed that cholesterol plays a fundamental role in membrane trafficking and signaling (Hurley and Meyer, 2001). Certain proteins bind to membranes in response to local changes in lipid composition that enhance or suppress their interactions with ligands or protein partners. Others have reported that cho-

The online version of this article includes supplemental material.

Address correspondence to Nobutaka Hirokawa, Department of Cell Biology and Anatomy, Graduate School of Medicine, University of Tokyo, 7-3-1 Hongo, Tokyo 113-0033, Japan. Tel.: 81-3-58413326. Fax: 81-3-5802-8646. E-mail: hirokawa@m.u-tokyo.ac.jp

*Abbreviations used in this paper: BFA, brefeldin A; CyDy, cytoplasmic dynein; KIF, kinesin superfamily protein; LPDS, lipoprotein-deficient serum; MT, microtubule; MTOC, microtubule organizing center; VSVG, vesicular stomatitis virus glycoprotein.

Key words: KIFC3; Golgi apparatus; cholesterol; dynein; microtubule

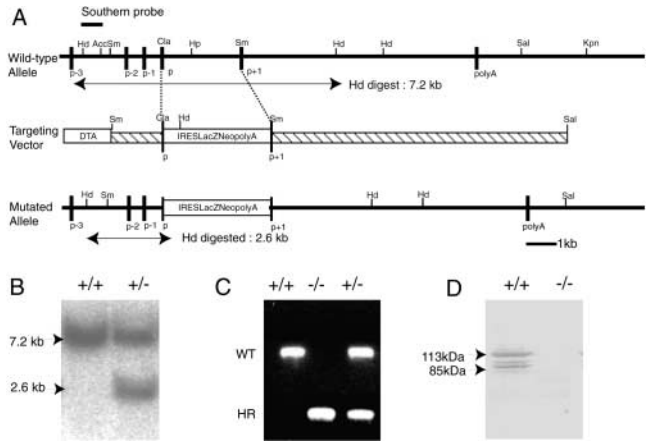

Figure 1. **Disruption of the mouse *kifC3* gene.** (A) Structures of wild-type *kifC3* gene (top), targeting vector (IRES, internal ribosome entry site; LacZ, β galactosidase gene; neo, promoterless neomycin resistance gene; polyA, RNA polymerase II pausing signal) (middle), and mutant *kifC3* gene after homologous recombination (bottom). Closed boxes, p−3, p−2, p−1, and p+1, respective exons around the p-loop. (B) Southern blot analysis of ES clones. Genomic DNA from ES cells was digested with HindIII and subjected to hybridization with the probe indicated in A. The knockout and wild-type alleles are detected as 7.2- and 2.6-kb bands, respectively (B, arrowheads). (C) PCR analysis of *kifC3* gene using mouse tail genomic DNA. HR, homologous recombinant band; WT, wild-type band. Genotypes: +/+, wild type; +/−, heterozygote; −/−, homozygote. (D) Immunoblots of total kidney homogenate from wild-type and null mutant mice using anti-KIFC3 antibody. The lower band is a truncated form of KIFC3. The specific bands of KIFC3 (arrowheads) are not detected in *kifC3*$^{-/-}$ kidney.

lesterol deprivation affects trafficking of vesicles that contain glycosylphosphatidylinositol proteins and sphingolipid–cholesterol rafts (Keller and Simons, 1998). Thus, we intended to modify the subcellular milieu by cholesterol deprivation to determine the specific function of KIFC3. Here, we provide evidence that KIFC3, together with CyDy, plays a definite role in Golgi integration and positioning under the cholesterol-depleted and normal conditions, using gene targeting combined with GFP and time-lapse imaging technology.

Results

Targeted disruption of the *kifC3* gene

We disrupted the mouse *kifC3* gene by using a promoter-trapping strategy (Figs. 1, A–C). A *lacZ* gene fused with the neopositive selection marker was knocked in to identify the tissues that express the KIFC3 protein. Complete disruption of the KIFC3 protein was confirmed by Western blotting with a specific antibody (Noda et al., 2001) (Fig. 1 D). *KifC3*-null mutants were normal in appearance, growth, and fertility. No obvious change was observed in the standard screening by histological analysis using light and electron microscopies (unpublished data), as reported by Yang et al. (2001).

KIFC3 was localized at the Golgi region in adrenocortical cells

We examined the tissue distribution of KIFC3 by knocked-in reactivity of galactosidase as well as by immunoblotting.

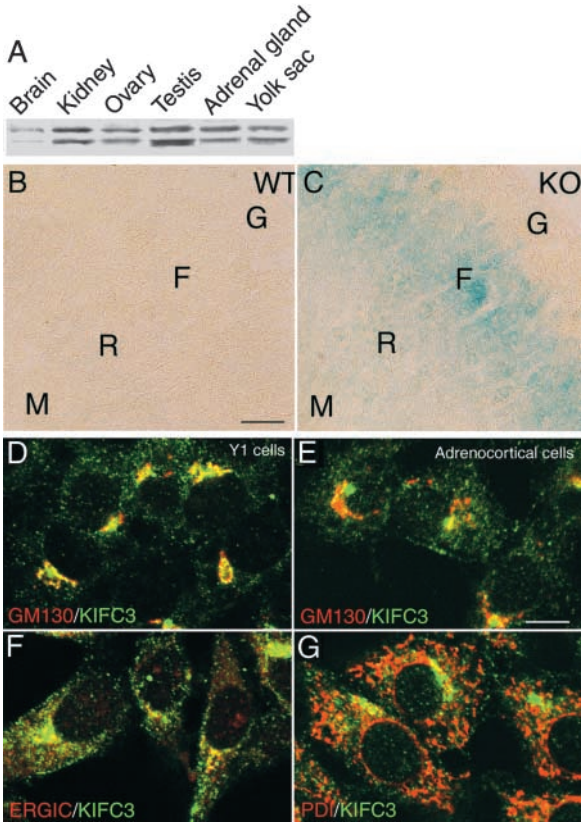

Figure 2. **Localization of KIFC3.** (A) Western blot analysis shows that KIFC3 is relatively abundant in the kidney, testis, adrenal gland, ovary, and yolk sac, but scanty in the brain. (B and C) A microscopic section of adrenal tissue stained against β-galactosidase. The adrenocortical area shows a strong signal of β-galactosidase. (B) Wild type; (C) knockout. G, zona glomerulosa; F, zona fasciculata; M, adrenal medulla; R, zona reticularis. Bar, 100 μm. Distribution of KIFC3 in Y1 cell line (D, E, and G) and primary adrenocortical cells (E). Merged image double-stained with anti-KIFC3 antibody (green) and antibodies (red) against GM130 (D and E), PDI (F), or ERGIC (G). Bar, 10 μm.

The expression of KIFC3 was ubiquitous (Noda et al., 2001), however, we found that KIFC3 was abundantly expressed in the kidney, testis, adrenal glands, ovary, and yolk sac (Fig. 2 A). The paraffin-embedded sections of the adrenal glands showed β-galactosidase staining that was particularly intense and limited to adrenal cortex cells (Fig. 2, B and C). Thus, we examined the subcellular localization of KIFC3 in adrenocortical cells by immunofluorescence. KIFC3 was localized mainly at perinuclear regions in the mouse adrenal cortex cell line (Y1) as well as in adrenocortical cells in primary culture (Fig. 2, D and E), although KIFC3 was localized in the apical subplasma membrane area in polarized MDCK cells (Noda et al., 2001). KIFC3 also has similar localization in cultured nonpolarized cells such as fibroblasts (unpublished data). The perinuclear expression pattern showed an extensive overlap with Golgi apparatus markers, such as GM130 (Fig. 2, D and E). In the perinuclear area of the cell, partial overlap of images was observed between ERGIC-53– and KIFC3-positive dotty structures (Fig. 2 F), but little overlap with ER marker (Fig. 2 G). This subcellular localization suggests that KIFC3 may be related to Golgi trafficking in these cells.

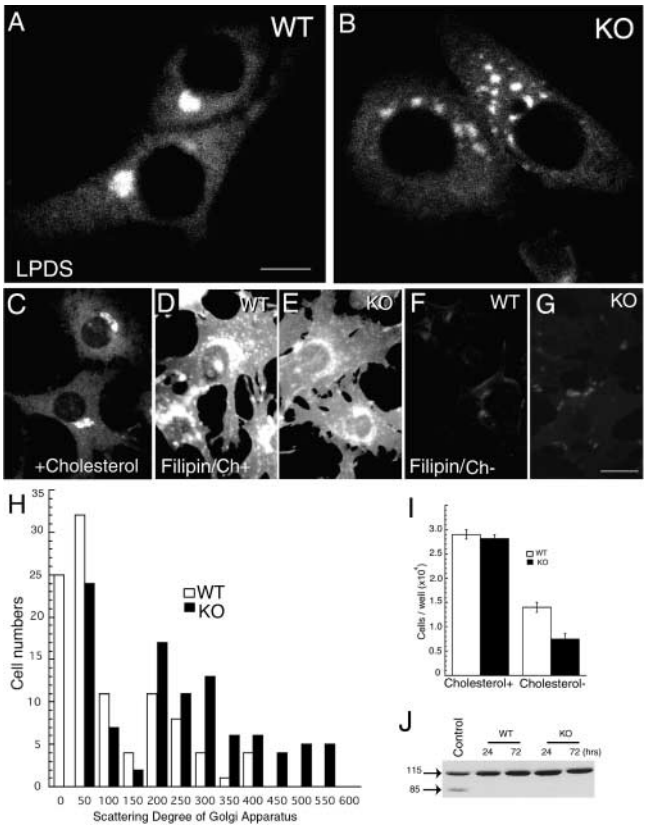

Figure 3. **Phenotype of Golgi apparatus in *kifC3*$^{-/-}$ adrenocortical cells under cholesterol-depleted condition.** (A and B) Golgi apparatus labeled with BODIPY-ceramide in LPDS medium. Golgi apparatus is stained as a compact perinuclear structure in wild-type cells (A), whereas it is fragmented around the nucleus in *kifC3*$^{-/-}$ cells (B). (C) Cholesterol-deprived *kifC3*$^{-/-}$ cells were replenished with cholesterol. The dispersed Golgi apparatus in *kifC3*$^{-/-}$ cells recovers its compact arrangement. (D–G) Filipin staining of adrenocortical cells grown in the presence (D and E) or absence of cholesterol (F and G). (D and F) Wild-type; (E and G) knockout. Cholesterol is completely depleted by treatment with LPDS. Bars, 10 μm. (H) Histogram of the scattering degree of Golgi fragments in 100 wild-type (open bars) and 100 *kifC3*$^{-/-}$ cells (solid bars). The distribution of the Golgi fragments in *kifC3*$^{-/-}$ cells is shifted to the higher scores ($p < 0.01$), indicating the dispersion of the Golgi apparatus in *kifC3*$^{-/-}$cells. (I) Comparison of the viability between wild-type and *kifC3*$^{-/-}$ cells in FCS and LPDS media after 72 h. Left and right panels display cells grown in the cholesterol^{+} and cholesterol^{-} medium, respectively, showing the lower viability of *kifC3*$^{-/-}$ cells in the latter medium. (J) Western blotting by anti-PARP antibody in wild-type and *kifC3*$^{-/-}$ cells cultured in LPDS medium for the indicated hours. Caspase-cleaved product (85 kD) shown in control apoptotic cells induced by TNF, was not detected in both cells grown in LPDS medium.

Golgi apparatus dispersed in *kifC3*$^{-/-}$ cells when deprived of cholesterol

In adrenocortical cells, the Golgi apparatus was located around the microtubule organizing center (MTOC), as visualized by double labeling with anti–γ-tubulin and anti–Rab6 antibodies (unpublished data). When the cells were cultured in a medium containing 10% FCS, the Golgi apparatus in *kifC3*$^{-/-}$ cells showed compact juxtanuclear distribution using BODIPY-ceramide staining. Interestingly, when *kifC3*$^{-/-}$ cells were cultivated for 1 d in a cholesterol-depleted medium that contained 5% lipoprotein-deficient serum (LPDS) and 0.2% BSA, the Golgi apparatus was fragmented around the nucleus to form a spotty distribution pattern (Fig. 3 B). When we replenished cholesterol by adding HDL to the medium, the dispersed fragments of Golgi apparatus in *kifC3*$^{-/-}$ cells recovered to the compact perinuclear pattern (Fig. 3 C). To verify the decrease in the cholesterol content of wild-type and *kifC3*$^{-/-}$ cells in the LPDS medium, we used filipin, a fluorescent polyene antibiotic reagent that forms specific complexes with cholesterol (Miller, 1984). Prominent labeling of the plasma membrane and the vesicular structure in the cytoplasm by filipin was observed when the cells were cultured in 10% FCS medium (Fig. 3, D and E). In contrast, after incubation in the LPDS medium for 1 d, staining of the plasma membrane almost completely disappeared and the cytoplasmic vesicular staining also decreased in both types of cells (Fig. 3, F and G). The Golgi apparatus fragmentation was further analyzed quantitatively using NIH image software. The scattering degree of Golgi apparatus fragments in *kifC3*$^{-/-}$ cells was significantly higher than that in wild-type cells ($p < 0.01$; $n = 100$) (Fig. 3 H), indicating that the dispersion of the Golgi apparatus fragments was significant in *kifC3*$^{-/-}$ cells. When we cultured the cells for a longer time (72 h), the viability of the *kifC3*$^{-/-}$ adrenocortical cells was significantly reduced in the LPDS medium compared with that of wild-type cells. However, no difference in viability was detected in FCS medium between the two groups (Fig. 3 I). To test whether the fragmentation of the Golgi apparatus was due to apoptosis (Lane et al., 2002), we examined the presence of caspase-cleaved PARP by a specific antibody. No cleavage products were detected, indicating that the Golgi fragmentation in *kifC3*$^{-/-}$ cells was independent of the apoptotic process (Fig. 3 J).

To test whether this condition affects the distribution of other organelles, we examined lysosomes and mitochondria and found their distribution pattern unchanged (unpublished data). To assess the molecular composition of the scattered fragments, anti-βCOP, mannosidase II, Rab6 antibodies, and TGN38–GFP vector were chosen to identify a subpopulation of Golgi membranes (Fig. 4, A–H). The dispersion patterns in *kifC3*$^{-/-}$ cells were similar among these markers, indicating that the fragments are Golgi stacks consisting of cis-, medial-, and trans-Golgi and TGN.

To further investigate ultrastructural changes in *kifC3*$^{-/-}$ adrenocortical cells due to cholesterol depletion, we compared wild-type and *kifC3*$^{-/-}$ cells by EM. In accordance with the result on the light microscopic level, the Golgi apparatus tended to be dispersed in *kifC3*$^{-/-}$ cells but compact in wild-type cells (Fig. 4, I and J). Nevertheless, these Golgi fragments existed in the form of stacks of cisternae (Fig. 4 K), indicating that even under the cholesterol-depleted condition, the Golgi apparatus is capable of forming stacks of cisternae.

Next, in order to rule out the possibility that these apparent fragments of the Golgi apparatus were connected with each other by a thin interconnecting membranous component that might have been overlooked by EM, we observed the diffusion of the BODIPY-ceramide stain through the membrane structure by the FRAP method (Fig. 4, L and M). After photobleaching of a limited area of the Golgi region, the BODIPY-ceramide stain was immediately recovered in wild-type cells (Fig. 4 L). In contrast, we did not ob-

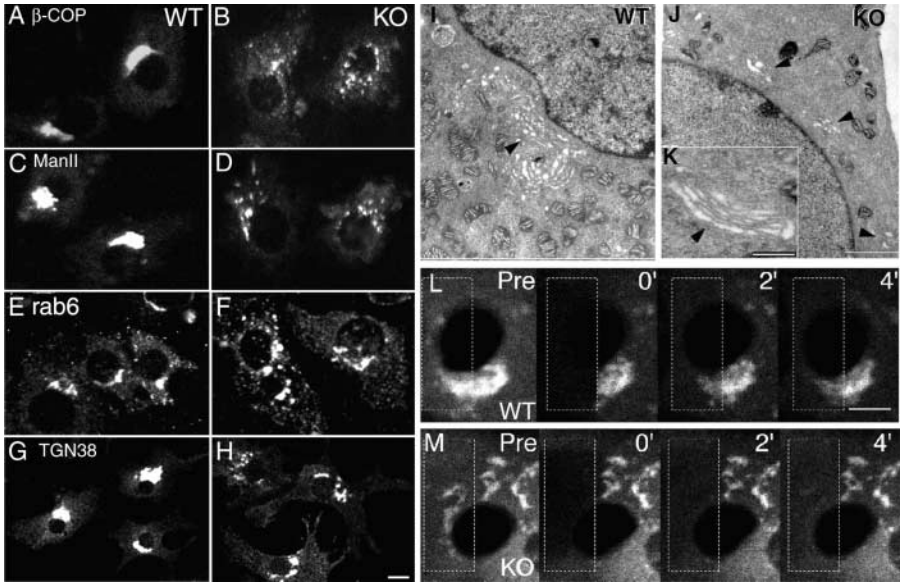

Figure 4. **Structure of the Golgi apparatus under cholesterol-depleted condition.** (A–F) Micrographs of the Golgi apparatus stained by antibodies against three different Golgi regions. β-COP (A and B), mannosidase II (C and D), Rab6 (E and F). (G and H) Adrenocortical cells expressing TGN38–GFP. All these proteins lose their juxtanuclear localization in *kifC3*$^{-/-}$ cells (B, D, F, and H) compared with those in wild-type cells (A, C, E, and G). Bar, 10 μm. (I–K) Electron micrographs of Golgi apparatus in wild-type (I) and *kifC3*$^{-/-}$ (J and K) cells after cholesterol deprivation. Arrowheads indicate the Golgi apparatus. Bar, 1 μm. (K) At higher magnification, a Golgi fragment clearly consists of several cisternal stacks in *kifC3*$^{-/-}$ cells. Bar, 500 nm. (L and M) Fluorescence recovery of BODIPY-ceramide after photobleaching of Golgi membranes followed by imaging at the times indicated. Note that fluorescence was recovered in the prebleached region in wild-type cells (L), but not in *kifC3*$^{-/-}$ cells (M), indicating that these fragments in *kifC3*$^{-/-}$ cells are discontinuous. Bar, 10 μm.

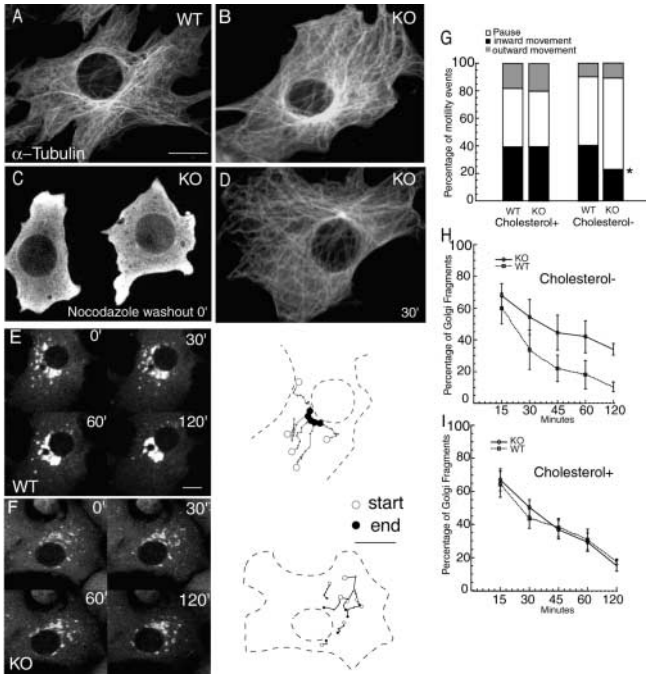

Figure 5. **Dynamics of Golgi fragments in wild-type and *kifC3*$^{-/-}$ cells after nocodazole removal under cholesterol-depleted condition.** (A–D) Distribution of MTs in wild-type (A) and *kifC3*$^{-/-}$ (B–D) cells stained by anti–α-tubulin antibody. The patterns of MTs are similar in both cells without treatment (A and B). Dispersed MTs after nocodazole removal (0 min; C) recovered within 30 min (D). (E and F) Time-lapse image of the Golgi apparatus in wild-type (E) and *kifC3*$^{-/-}$ (F) cells after nocodazole washout. Right panels show several accumulated Golgi fragment tracks from start to end in wild-type (upper) and *kifC3*$^{-/-}$ (lower) cells (see Videos 1 and 2, available at http://www.jcb.org/cgi/content/full/jcb.200202058/DC1). Bars, 10 μm. (G) Quantitative analysis of assembly movement of Golgi fragments in the presence and absence of cholesterol after nocodazole washout. The proportion of outwardly directed movements, stop, and inwardly directed movements of Golgi fragments was evaluated for each fluorescent spot after nocodazole washout in the cholesterol^{+} and cholesterol^{-} medium in wild-type (WT) and *kifC3*$^{-/-}$ (KO) cells, respectively. Each column shows the average proportion of 100 spots in 10 cells of each group. The degree of inwardly directed motility is markedly reduced in *kifC3*$^{-/-}$ cells only in the cholesterol^{-} medium ($p < 0.01$). (H and I) The kinetics of reassembly of the Golgi apparatus in the absence (H) and presence (I) of cholesterol medium. The number of fragments per cell was defined by counting spots that contained more than four pixels in size. The y axis shows percentage of the total numbers of Golgi fragments at their respective time divided by the number of the Golgi fragments after nocodazole washout at 0 min.

serve the recovery in a bleached region of *kifC3*$^{-/-}$ cells (Fig. 4 M), suggesting that Golgi fragments in *kifC3*$^{-/-}$ cells are independent of each other and not connected by membranous components.

Cholesterol depletion decreased inwardly directed movement of Golgi fragments in *kifC3*$^{-/-}$ cells

In our previous report, we showed that KIFC3 is a MT minus end–directed motor (Noda et al., 2001). Considering that the Golgi apparatus is localized around the MTOC in adrenocortical cells, integration of Golgi fragments is supposed to be conveyed by MT minus end–directed motors, which suggests the possibility that the phenotype of Golgi dispersion is due to the lack of minus end–directed motility by the KIFC3 protein. To test this hypothesis, we first confirmed that MT organization was still preserved in both types of cells under the cholesterol-depleted condition (Fig. 5, A and B). Next, to visualize the movement of Golgi fragments, we performed two perturbation experiments. One involved nocodazole treatment, and the other involved brefeldin A (BFA) administration.

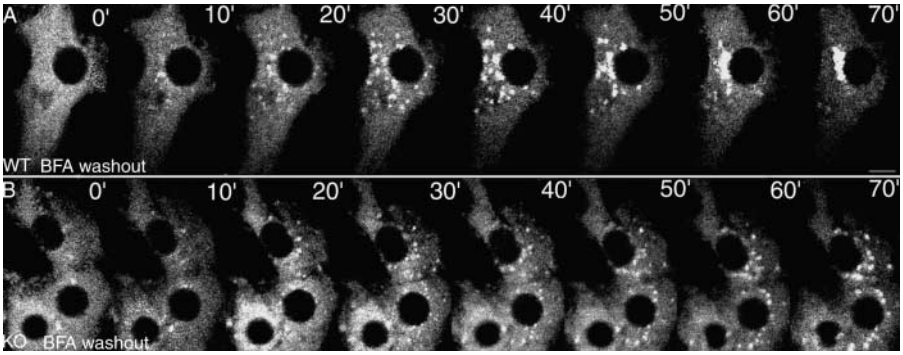

Figure 6. **Time-lapse images of recovery of the Golgi apparatus after BFA treatment under cholesterol-depleted condition.** (A and B) Representative time-lapse images from 0 to 70 min. The Golgi apparatus is distributed homogeneously throughout the cytoplasm after BFA treatment in wild-type (0′) and *kifC3*$^{-/-}$ (0′) cells. After 70 min of incubation without BFA, almost all the fragments concentrated near the MTOC in wild-type cells (top row), whereas many smaller Golgi fragments were still dispersed in the cytoplasm in *kifC3*$^{-/-}$ cells (bottom row). The time-lapse videos are available at http://www.jcb.org/cgi/content/full/jcb.200202058/DC1 (Videos 3 and 4). Bar, 10 μm.

In the first experiment, cells were incubated with 33 μM nocodazole, which completely depolymerized the MTs. After the nocodazole washout, the MTs restored their original arrangement within 30 min, which enabled us to monitor the recovery movement of the dispersed Golgi fragments along the MTs toward the cell center (Ho et al., 1989; Cole et al., 1996). As for MTs, the recovery process in *kifC3*$^{-/-}$ cells was similar to that in wild-type cells (Fig. 5, C and D). After the nocodazole treatment, the Golgi fragments were dispersed throughout the cytoplasm, showing that intact MTs are indispensable for proper positioning of the Golgi apparatus in both types of cells. The time-lapse of the recovery phase of Golgi membranes after the nocodazole washout was observed in wild-type and *kifC3*$^{-/-}$ cells under the cholesterol-depleted condition (Fig. 5, E and F). Because of the flatness of these cells, >90% of all Golgi fragments in the cells could be observed in a single focal plane. Generally, 30–60 Golgi fragments were identified in a single cell after drug treatment. In cholesterol-depleted wild-type cells, Golgi fragments clearly showed a centripetal movement along linear tracks consistent with MTs. Reassembly of the Golgi apparatus in the vicinity of the MTOC was completed within 120 min (Fig. 5 E; see Video 1, available at http://www.jcb.org/cgi/content/full/jcb.200202058/DC1). In cholesterol-depleted *kifC3*$^{-/-}$ cells, on the other hand, the Golgi fragments exhibited a sluggish movement. After 120 min, the Golgi fragments still remained dispersed although the MTs had fully reassembled (Fig. 5 F; Video 2).

To quantify these data, we performed the following approaches. First, we quantified the Golgi recovery movement by following the fluorescent spot movement stained by BODIPY-ceramide. 100 spots each from 10 different cells of each cell type were selected. For analysis, movement away from the cell center was indicated as outwardly directed motility, and movement toward the cell center as inwardly directed motility. Movement of the spots was bidirectional in both types of cells. They did not move to the MTOC incessantly, but they sometimes made turns and moved backward. The net displacements within 120 min were inwardly directed in both types of cells. However, their patterns of movements were different. The frequency of inwardly directed movement in wild-type cells was significantly higher (40.6%) than that in *kifC3*$^{-/-}$ cells (22.8%; $p < 0.01$) (Fig. 5 G). This is consistent with the property of KIFC3, being a minus end–directed motor protein. There were no significant differences in MT outwardly directed movement. The maximum run length was not affected by disruption of the *kifC3* gene (2.5 ± 0.25 vs. 2.2 ± 0.39 μm). Finally, we compared the kinetics of Golgi reassembly between both cell types (Fig.5, H and I). In the case of wild-type cells, 78% of the scattered Golgi fragments were assembled near the MTOC within 30 min, increasing to 90% in 120 min. In contrast, *kifC3*$^{-/-}$ cells exhibited a 56% recovery in 30 min ($p < 0.001$) and 66% in 120 min, though they gathered in the perinuclear area ($p < 0.001$) (Fig. 5 H). This difference was not observed when the cells were grown in 10% FCS medium (Fig. 5 I).

In the second experiment, adrenocortical cells were treated with BFA, which caused the disappearance of the central Golgi apparatus by facilitating the backward transport to the ER (Lippincott-Schwartz et al., 1989). Because BFA does not affect MT organization, ER-to-Golgi transport can be monitored immediately after the removal of BFA. There was no difference in drug sensitivity to BFA between both cell types. After the removal of BFA, in wild-type cells, a number of ceramide-labeled spots became visible within the cytoplasm at 20 min (Fig. 6 A), which made rapid centripetal movements along linear tracks, implying the existence of MTs even under the cholesterol-depleted condition (Video 3). Finally, they fused to form a compact perinuclear Golgi complex. In cholesterol-depleted *kifC3*$^{-/-}$ cells, the labeled spots also became visible at 20 min and moved to the central area after BFA washout. However, they failed to reconstitute the compact Golgi complex (Fig. 6 B). Although these small spots, observed at first in *kifC3*$^{-/-}$ cells, had a size, shape, and fluorescence intensity similar to those in wild-type cells, they continued oscillatory movements with a shorter cycle even at 70 min (Video 4). To address whether this difference was due to a lack of inwardly directed motility, the dynamics of Golgi fragments was analyzed in detail (Table I). The frequency of the inwardly directed motility was decreased in *kifC3*$^{-/-}$ cells ($p < 0.01$). Furthermore, the amount of fragments travelling a long distance (>2 μm) was significantly reduced. These data collec-

Table I. **Movement of Golgi fragments after BFA removal in wild-type and *kifC3*$^{-/-}$ cells**

	WT	KO
	%	%
Outward motility events	9.19 ± 3.24	16.87 ± 3.90[a]
Inward motility events	53.03 ± 8.35	29.3 ± 4.32[a]
Displacement >2μm	47.9 ± 8.02	18.03 ± 3.50[a]

Behavior of Golgi fragments in wild-type and *kifC3*$^{-/-}$ cells after BFA washout under the cholesterol-depleted condition. The percentages of outwardly and inwardly directed motility events were calculated in wild-type and *kifC3*$^{-/-}$ cells. The values are expressed as means ± SD.
[a]$p < 0.01$.

tively account for the disorganized morphology of the Golgi apparatus in *kifC3*$^{-/-}$ cells under the cholesterol-depleted condition.

To exclude the secondary effects of chronic cholesterol depletion induced by 1-d culture in the LPDS medium, we examined the effect of subacute cholesterol efflux on Golgi trafficking. We treated cells with methyl β-cyclodextrin, which selectively and rapidly reduces the intracellular cholesterol content (Kilsdonk et al., 1995), and examined the Golgi recovery process after nocodazole washout (Fig. 7). As expected, the reassembly of the Golgi apparatus fragments near the MTOC was obviously delayed in *kifC3*$^{-/-}$ cells compared with that in wild-type cells. At 120 min after the nocodazole washout, 80 ± 7.6% of wild-type cells showed a compact Golgi apparatus (Fig. 7 B), versus 15 ± 6% of *kifC3*$^{-/-}$ cells ($p < 0.01$; Fig. 7 D), indicating that subacute cholesterol efflux also disturbed the Golgi assembly process in *kifC3*$^{-/-}$ cells. These findings, combined with our cholesterol rescue experiment, suggest that KIFC3 and cholesterol play a complementary role in Golgi positioning and integration.

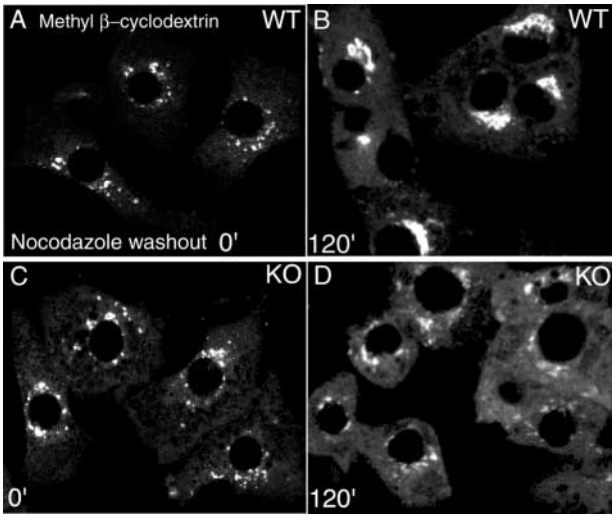

Figure 7. **Recovery of the Golgi apparatus after nocodazole treatment under subacute cholesterol-depleted condition.** After a 120-min incubation with methyl β-cyclodextrin in the LPDS medium, followed by nocodazole treatment, the Golgi apparatus is diffusely distributed in both wild-type (A) and *kifC3*$^{-/-}$ (C) cells. At 120′ after nocodazole washout, compact Golgi apparatus appeared in wild-type cells (B), whereas a fragmented one was observed in *kifC3*$^{-/-}$ cells (D).

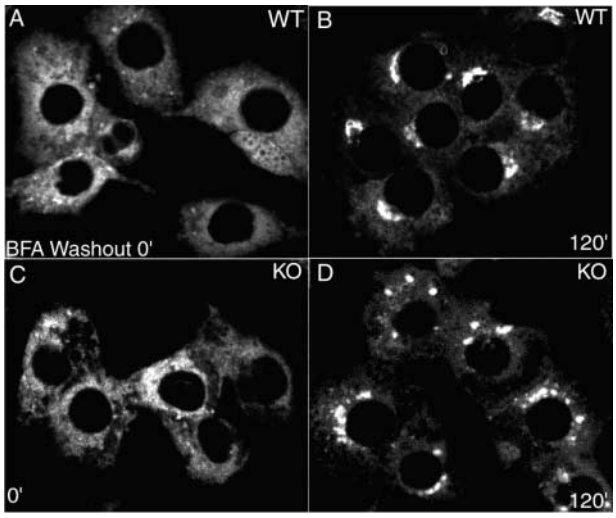

Figure 8. **Recovery process after BFA washout in the presence of cytochalasin D under cholesterol-depleted condition.** The recovery processes of the Golgi apparatus labeled with BODYPY-ceramide after BFA treatment were observed in wild-type (A and B) and *kifC3*$^{-/-}$ (C and D) cells in the presence of 1 μM cytochalasin D. The images were recorded at the indicated times after BFA removal, showing no change compared with those without cytochalasin D (Fig. 6).

To examine the involvement of actin in the observed Golgi morphological changes in *kifC3*$^{-/-}$ cells, we studied the recovery processes after BFA treatment in the presence of cytochalasin D. The recovery processes were similar to those in the absence of cytochalasin D (compare Fig. 8 with Fig. 6), suggesting that Golgi dispersion in *kifC3*$^{-/-}$ cells is independent of the actin-based cytoskeletal network.

KIFC3 had no effect on the kinetics of ER-to-Golgi transport

To exclude the possibility that the observed difference was due to the change in the structure of the ER, immunofluorescence staining was employed for visualizing the morphology of the ER, which showed no marked difference in shape (unpublished data). To further investigate at which stage KIFC3 functions in Golgi positioning and integration, we employed the GFP fusion protein containing a temperature-sensitive mutant of the vesicular stomatitis virus glycoprotein (VSVG) (Presley et al., 1997) (Fig. 9). At a nonpermissive temperature (39.5°C), vesicular trafficking is blocked at the ER, whereas shifting the temperature to 30°C (permissive temperature) restarts ER-to-Golgi trafficking. In both types of cells in the LPDS medium, VSVG–GFP was completely redistributed into the Golgi region within 5 min after the temperature shift from 39.5°C to 30°C (Fig. 9, A–D; Video 5). The kinetics of VSVG–GFP upon translocation to the Golgi region was quantified by measuring the relative fluorescence intensity at various time points (Zaal et al., 1999), and similar profiles of transport in both types of cells were obtained (Fig. 9, K and L). These data suggest that in spite of the Golgi fragmentation phenotype of *kifC3*$^{-/-}$ cells, VSVG–GFP was transported to the Golgi region as ef-

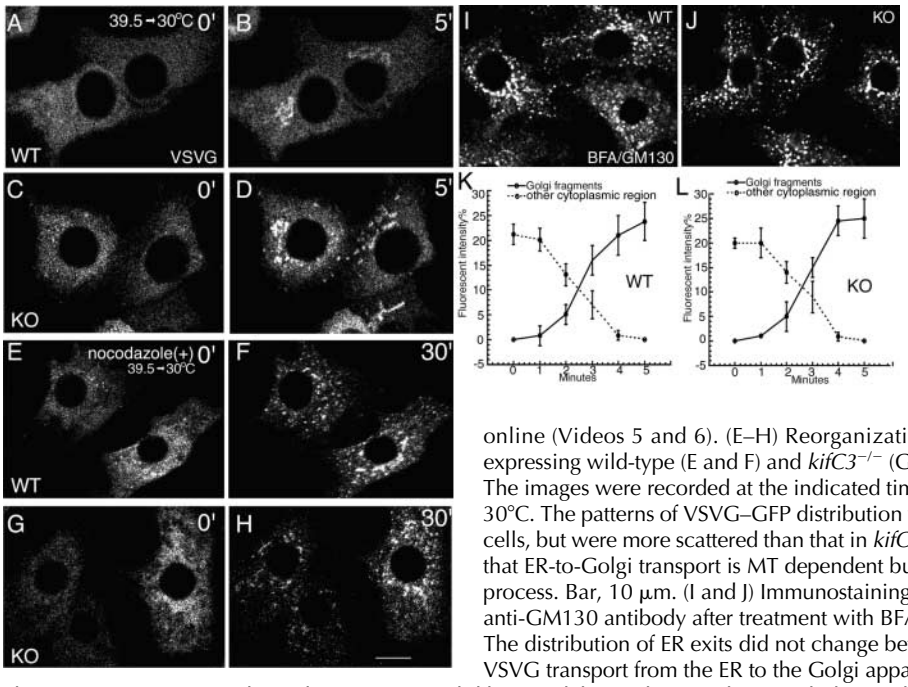

Figure 9. **ER-to-Golgi transport of VSVG–GFP in wild-type and *kifC3*$^{-/-}$ cells under cholesterol-depleted condition.** (A–D) ER-to-Golgi transport of VSVG–GFP in wild-type (A and B) and *kifC3*$^{-/-}$ (C and D) cells. Wild-type and *kifC3*$^{-/-}$ cells expressing VSVG–GFP were incubated at 39.5°C for 6 h (A and C), and then the temperature was shifted to 30°C for 5 min (B and D) in LPDS medium. Note that VSVG accumulated in the corresponding Golgi apparatus area within 5 min in *kifC3*$^{-/-}$ cells as efficiently as in wild-type cells, although the Golgi apparatus was dispersed in *kifC3*$^{-/-}$ cells. Video images are available online (Videos 5 and 6). (E–H) Reorganization of the Golgi apparatus in VSVG–GFP-expressing wild-type (E and F) and *kifC3*$^{-/-}$ (G and H) cells in the presence of nocodazole. The images were recorded at the indicated times after the temperature shift from 39.5°C to 30°C. The patterns of VSVG–GFP distribution were similar in wild-type (F) and *kifC3*$^{-/-}$ (H) cells, but were more scattered than that in *kifC3*$^{-/-}$ cells without nocodazole (D), indicating that ER-to-Golgi transport is MT dependent but not coincident with the KIFC3-dependent process. Bar, 10 μm. (I and J) Immunostaining of wild-type (I) and *kifC3*$^{-/-}$ (J) cells with anti-GM130 antibody after treatment with BFA under the cholesterol-depleted condition. The distribution of ER exits did not change between the two groups. (K and L) Kinetics of VSVG transport from the ER to the Golgi apparatus in wild-type (I) and *kifC3*$^{-/-}$ (J) cells. Fluorescence intensity in the Golgi apparatus (solid line) and that in the cytoplasm excluding Golgi region (dotted line) were quantified at the indicated times in wild-type (K) and *kifC3*$^{-/-}$ (L) cells. No difference is observed between the two groups.

ficiently as in the wild-type cells. When we observed VSVG–GFP dynamics in the presence of nocodazole in the LPDS medium, VSVG–GFP was accumulated to small spots distributed throughout the cytoplasm in both wild-type and *kifC3*$^{-/-}$ cells (Fig. 9, F and H; Video 6). The pattern is totally different in terms of spot size, spot number, and appearance from those without nocodazole in *kifC3*$^{-/-}$ cells in the LPDS medium (Fig. 9, compare H with D; compare Video 6 with Video 5). We further checked the distribution of the ER exit sites in the cholesterol-depleted condition by the redistribution of GM130 to the ER exit sites after BFA treatment, as described in Ward et al. (2001), which showed no change between the two types of cells (Fig. 9, I and J).

KIFC3 and cytoplasmic dynein cooperated in the positioning of the Golgi apparatus

In this study, we demonstrated that KIFC3 is essential for the assembly of the Golgi apparatus when deprived of cholesterol. However, disruption of the dynein gene was reported to cause disassembly of the Golgi apparatus (Harada et al., 1998). How can we explain the relationship between KIFC3 and the CyDy motor in Golgi positioning and integration? If the two motors work in combination, then the Golgi structure would become more sensitive to the inactivation of CyDy in *kifC3*$^{-/-}$ cells than in wild-type cells even in the presence of cholesterol. To test this hypothesis, we employed an adenovirus vector system with dynamitin fused to CFP to block CyDy function and evaluated the effects of KIFC3 on Golgi positioning and integration. We controlled the amount of exogenous dynamitin–CFP through infection of cells within a suitable length of time by checking the fluorescence intensity of CFP (Burkhardt et al., 1997). The expression rates of dynamitin–CFP were similar between wild-type and *kifC3*$^{-/-}$ cells (after a 12-h infection, the fluorescence intensity was 77 ± 17 U in wild-type cells and 78 ± 17 U in *kifC3*$^{-/-}$ cells). Dynamitin expression after a 12-h infection caused dispersion of the Golgi apparatus labeled with BODIPY-ceramide in 83 ± 6% of wild-type cells and in 85 ± 5% of *kifC3*$^{-/-}$ cells (Fig. 10, E–G). However, when we observed the cells after a 6-h infection, more *kifC3*$^{-/-}$ cells (80 ± 8.2%) showed a dispersed Golgi pattern compared with wild-type cells (35 ± 6.7%) ($p < 10^{-7}$) (Fig. 10, C, D, and G), although the average fluorescence intensity of dynamitin–CFP showed no difference (unpublished data). The level of dynamitin–CFP per cell was classified and compared between both groups. When the fluorescence intensity was between 30 and 60 U, 82.7% of *KifC3*$^{-/-}$ cells showed a diffuse dispersion pattern of Golgi apparatus, versus 47.56% in wild-type cells (Fig. 10, H and I). In wild-type cells, we observed the same extent of fragility of Golgi apparatus against dynamitin expression, irrespective of the level of cholesterol in the medium (Fig. 10 G), suggesting that the effects of dynamitin and cholesterol depletion are not additive.

Thus, the following question arises: why was the phenotype of *kifC3*$^{-/-}$ cells observed only when cholesterol was depleted? We first examined the possibility that CyDy was released from the membrane under the cholesterol-depleted condition. However, CyDy in the membrane fraction did not change significantly between cells in FCS and LPDS medium (Fig. 10 J). The differential detergent extraction method, described by Hollenbeck (1989), revealed that the amount of CyDy detected in the vesicle fraction (saponin-insolubilized but triton-solubilized fraction) decreased significantly after growth in LPDS medium for 24 h (Fig. 10 K). In contrast, the amount of KIFC3 in the same fraction was not altered by cholesterol depletion (Fig. 10 K). Consid-

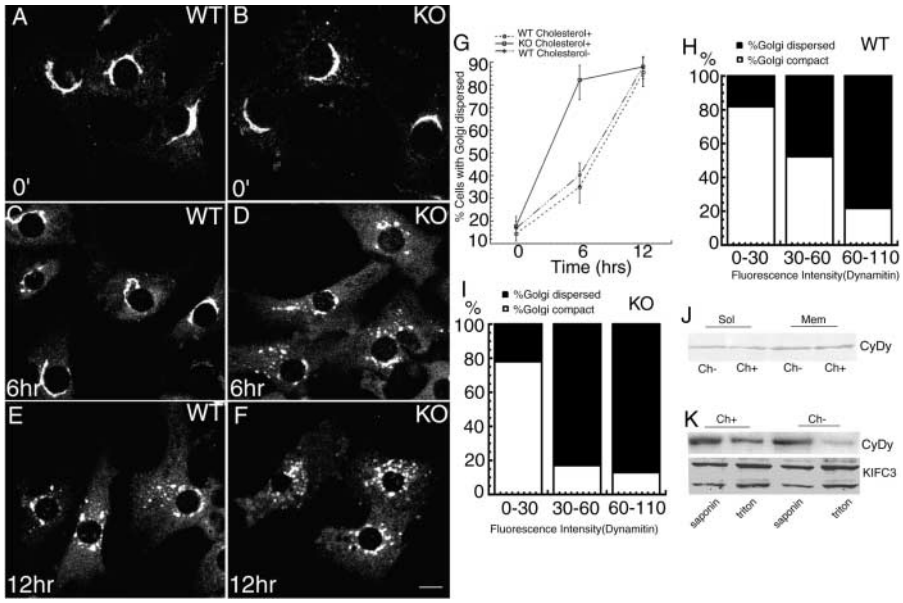

Figure 10. **Effects of dynamitin overexpression on the structure of the Golgi apparatus in wild-type and *kifC3*$^{-/-}$ cells.** Wild-type (A, C, and E) and *kifC3*$^{-/-}$ (B, D, and F) cells were observed at 0′ (A and B), 6 h (C and D), and 12 h (E and F) after the infection of adenovirus expressing dynamitin–CFP in FCS medium. The Golgi apparatus was labeled with BODIPY-ceramide at the indicated times. Dynamitin overexpression caused the dispersion of Golgi apparatus after a 12-h infection in both wild-type (E) and *kifC3*$^{-/-}$ (F) cells. After a 6-h infection, overexpression of dynamitin affected the Golgi apparatus more severely in *kifC3*$^{-/-}$ cells (D) than in wild-type cells (C). Bar, 10 μm. (G) Time course of the percentage of cells with dispersed Golgi pattern in wild-type (solid line) and *kifC3*$^{-/-}$ (dotted line) cells in cholesterol^{+} medium and wild-type cells in cholesterol^{-} medium (broken line). (H and I) Histogram of the percentage of cells with dispersed (solid box) or compact (open box) Golgi apparatus is shown according to the fluorescence intensity of CFP–dynamitin after a 6-h infection (H, wild-type; I, *kifC3*$^{-/-}$ cells). Note that *kifC3*$^{-/-}$ cells are more susceptible to the intermediate level of dynamitin–CFP expression (30–60 U) than wild-type cells. (J) Subcellular fraction of CyDy in Y1 cells grown in cholesterol^{-} (lanes 1 and 3) or cholesterol^{+} (lanes 2 and 4) medium. No change is detected in the amount of soluble (lanes 1 and 2) as well as membrane-bound CyDy (lanes 3 and 4). (K) Immunoblot of CyDy and KIFC3 in detergent-extracted fraction of Y1 cells cultured in cholesterol^{+} or cholesterol^{-} medium. CyDy and KIFC3 were immunoprecipitated from fractions successively extracted by 0.02% saponin and 1% Triton X-100. CyDy in the Triton X-100–extracted fraction decreased in cholesterol^{-} medium, whereas KIFC3 did not change.

ering that the total amount of membrane-bound CyDy in the subcellular fraction did not change by the cholesterol depletion, more CyDy was supposed to be released from vesicle membranes by the preceding saponin extraction in cholesterol-depleted cells. These data suggest that the binding state of CyDy to its cargoes may be regulated by the cholesterol perturbation, and KIFC3 may be less influenced by cholesterol. This result may explain why KIFC3 is essential for Golgi assembly and integration only when cholesterol is depleted.

Discussion

The major points of interest in this study are as follows. (a) Targeting disruption of the *kifC3* gene showed abnormal fragmentation of the Golgi apparatus under the cholesterol-depleted condition, indicating that KIFC3 is required for Golgi integration and positioning. (b) The Golgi apparatus position is not solely determined by a single MT minus end–directed motor, but also by the balance between a plus end–directed motor protein(s) and at least two minus end–directed motor proteins (KIFC3 and CyDy). (c) KIFC3 and cholesterol play complementary roles in Golgi positioning and integration, revealing a novel regulatory mechanism of cholesterol in membrane trafficking. Additionally, this study also showed the importance of careful analysis of knockout mice. Frequently, knocking out a single gene results in a subtle phenotype, as reported previously (Harada et al., 1994; Yang et al., 2001). However, this does not necessarily mean that the gene is nonfunctional. As shown by previous double knockout studies (Takei et al., 2000; Teng et al. 2001) and this study, multiple proteins sometimes perform fundamental functions synergistically. This finding can only be elucidated by careful and detailed analysis of gene knockout mice.

Coordination of multiple motor proteins for Golgi assembly

It has been established that CyDy is a motor for locating the Golgi complex to the perinuclear area (Burkhardt et al., 1997; Presley et al., 1997; Harada et al., 1998). However, the present study revealed that KIFC3 is also involved in this process. In the Golgi reassembly experiments, we found that although Golgi fragments assembled into 5–10 larger fragmented Golgi apparatus that were distributed around the nucleus, they failed to further assemble into the compact structure in the absence of both KIFC3 and cholesterol. We do not exclude the possibility that cholesterol depletion may affect the membrane fusion. Our detailed quantitative analysis of individual movements of the dispersed Golgi apparatus revealed a decreased frequency of the inwardly directed motility in *kifC3*$^{-/-}$ cells compared with that in wild-type cells under the cholesterol-depleted condition, which strongly suggests that defects in Golgi motility result in the observed Golgi fragmentation phenotype. Furthermore, we obtained evidence that KIFC3 and CyDy work synergically to assemble the Golgi apparatus under the cholesterol-sufficient condition. In adrenocortical cells overexpressing proper levels of dynamitin, the Golgi structures showed much greater dispersion in *kifC3*$^{-/-}$ cells than in wild-type cells (Fig. 10). Obviously, CyDy can complete the assembly of the Golgi apparatus by itself under the cholesterol-sufficient condition; this does not necessarily mean that the motile effect of KIFC3 is restricted under the cholesterol-depleted condi-

tion. KIFC3 can be functional under either condition and becomes indispensable for the completion of the Golgi assembly especially under the cholesterol-depleted condition.

A recent study has revealed that the organization and localization of the mitotic spindle are determined by the coordination of activities of multiple motors (Stearns, 1997). Our results indicate that the position of the Golgi apparatus is also determined by a balance between multiple plus and minus end–directed motors, which is known as a "tug-of-war" mechanism. If motors that move toward the MT plus ends were dominant on the Golgi apparatus, it would be driven away from the cell center and become dispersed. Likewise, if minus end–directed motors were dominant, the Golgi apparatus would reside near the cell center, where MT minus ends converge. The phenotype of our *kifC3*$^{-/-}$ cells clearly indicates that the dynamic equilibrium of the Golgi apparatus is mediated by the balance between outward force driven by plus end–directed KIFs and the inward force driven by KIFC3 and CyDy. After the position of the Golgi apparatus is established, it may be linked to MTs via nonmotor components such as Golgi microtubule–associated proteins (Infante et al., 1999). As for the plus end–directed movement, recent biochemical and genetic studies identify several KIFs that are implicated in the Golgi membrane dynamics, such as Rab kinesin 6 and kinesin II/Xklp3/KIF3C (Echard et al., 1998). Further studies using knockout mice will reveal the plus end–directed motor proteins that balance with KIFC3 and CyDy for Golgi apparatus positioning.

Role of cholesterol in regulating motor proteins and organelle targeting

Our results demonstrate that cholesterol plays a key role in regulating motor proteins for Golgi apparatus positioning. Reduction in the level of cellular cholesterol caused the Golgi fragmentation in *kifC3*$^{-/-}$ cells (Fig. 3 B), and replenishment of cholesterol to the culture media rescued the Golgi phenotype (Fig. 3 C). Subacute cholesterol efflux studies using methyl β-cyclodextrin also showed the same results (Fig. 7). These results provide strong evidence that cholesterol is required for the effective positioning of the Golgi apparatus in *kifC3*$^{-/-}$ cells. This leads to two important conclusions. (1) Under the cholesterol-depleted condition, KIFC3 plays an essential role in organizing the Golgi structure. (2) Cholesterol is another important factor for organizing the fragmented Golgi stacks together into a compact structure. Our results also suggest that the function of the dynein–dynactin complex in Golgi assembly may be influenced by the amount of cholesterol in adrenocortical cells. This effect is specific to the Golgi assembly process, because our present data showed normal transport of intermediate vesicles to the Golgi fragments via CyDy in cholesterol-depleted *kifC3*$^{-/-}$ cells. Our previous work has also failed to detect the decrease in the level of CyDy in post-TGN vesicles in MDCK cells after cholesterol depletion (Noda et al., 2001). We think that partial detachment of the CyDy molecule from the membrane makes it difficult to move relatively larger stacks, such as fragmented Golgi stacks, but the remaining CyDy may be sufficient to transport small membranous structures such as transport complexes or post-TGN vesicles. The small decrease in the level of CyDy on the Golgi or post-TGN vesicles might be difficult to detect by immunostaining in this (Fig. 10 J) and our previous studies. The discrepancy of the results on the amount of membrane-bound CyDy in fractionation and after detergent extraction is consistent with the previous report by Lin et al. (1994), which may reflect the change in the quality of binding between CyDy and the membrane.

The present results also suggest that the cholesterol-dependent effect seems specific to CyDy, and the minus end–directed transport activity of KIFC3 is not affected by the perturbation of cholesterol. This might seemingly be contradictory to our previous result that acute efflux of cholesterol by methyl β-cyclodextrin destroyed the accumulation of KIFC3 beneath the apical plasma membrane of polarized MDCK cells (Noda et al., 2001). Indeed, this result can be interpreted as the binding of KIFC3 to its cargo vesicles and/or its transport being dependent on the intracellular cholesterol pool. However, as other studies already reported (Hanada et al., 1995; Keller and Simons, 1998), what actually happens in the polarized MDCK cells is the depletion or clearance of apically targeted post-TGN vesicles or "raft" vesicles, which are the main cargoes of KIFC3 in these cells. Thus, our previous experiments cannot clarify whether KIFC3′s activity is regulated by cholesterol or not, because the cholesterol depletion destroys the cargo itself in polarized epithelial cells. In adrenocortical cells analyzed in this study, the main cargo of KIFC3 is the Golgi complex, whose existence is not affected by the intracellular cholesterol level. Therefore, we can first conclude that KIFC3′s activity for the transport of the Golgi apparatus is not affected by the intracellular cholesterol level. This suggests that the transport activity of post-TGN apical vesicles by KIFC3 is also not primarily dependent on the intracellular cholesterol level, and the apparent loss of KIFC3 accumulation beneath the apical plasma membrane after methyl β-cyclodextrin treatment might be the secondary effect of the depletion of post-TGN apical vesicles.

Discoveries in the past 5 yr suggest that the composition of membrane cholesterol is important in the redistribution of membrane proteins (De Camilli et al., 1996; Kobayashi et al., 1999), raft trafficking (Keller and Simons, 1998), caveola transport (Hailstones et al., 1998), and signal transduction (Hurley and Meyer, 2001). Therefore, it is quite reasonable to assume the involvement of cholesterol in coordinating the proper orientation of the Golgi apparatus. We have established that KIFC3 and cholesterol maintain Golgi integration and positioning and that CyDy by itself is insufficient to generate a compact Golgi apparatus under the cholesterol-depleted condition. The next important question will be how the Golgi membrane or CyDy motility is regulated by cholesterol. Recent studies revealed that dynein association with membrane cargoes is regulated by the dynactin complex through interaction with spectrin (Schroer, 2000; Holleran et al., 2001). Further experiments are still necessary to determine the exact mechanism by which cholesterol regulates motor proteins.

Adrenocortical cells utilize cholesterol for synthesizing corticosteroid hormones that are necessary for the maintenance of homeostasis. Under severe conditions, such as starvation, there might be a possibility that these cells could

continue to produce abundant steroid hormones in spite of insufficient cholesterol supply and production. In such cases, the observed salvage pathway of Golgi assembly by KIFC3 might be necessary for species survival.

Materials and methods

Gene targeting of *KifC3*

Mouse genomic *kifC3* clones were isolated from a λEMBL3 genomic library of the ES cell line J1 as described previously (Harada et al., 1998). A region spanning the p-loop exon was replaced by the IRES-LacZ-neopA cassette inserted between the SmaI and ClaI sites, and the routine knockout procedures were performed according to the method of Harada et al. (1998).

Primary culture and treatment of adrenocortical cells

Adrenocortical cells were cultured as described by Ramachandran and Suyama (1975). For cholesterol deprivation, the cells were maintained in the D-Val medium containing 5% LPDS (Sigma-Aldrich) and 0.2% BSA (Sigma-Aldrich) for 1 d. To depolymerize MTs, cells were incubated with 33 μM nocodazole (Sigma-Aldrich) for 30 min on ice during incubation with BODIPY-ceramide followed by a 30-min incubation in serum-free MEM containing nocodazole at 37°C. Alternatively, cells were treated with 10 μg/ml BFA for 20 min, washed, and incubated for the indicated times. Under subacute cholesterol-depleted condition, methyl β-cyclodextrin (10 mM; Sigma-Aldrich) was added to the LPDS medium 2 h before BODIPY-ceramide staining and nocodazole treatment. In actin studies, cytochalasin D (1 μM; Sigma-Aldrich) was added during the recovery process.

Immunohistochemistry and immunoblotting

Immunoblotting and immunohistochemistry were performed as described previously (Harada et al., 1998). For the first antibodies, the following antibodies were used: anti-ERGIC-53 (a gift from H.P. Hauri, University of Basel, Basel, Switzerland) (Schweizer et al., 1988); anti–α-tubulin and anti–β-COP antibodies (Sigma-Aldrich); anti–Rab6 (Santa Cruz Biotechnology, Inc.); anti-GM130 (Transduction Labs); anti–poly-ADP-ribose polymerase (PARP; Oncogene Research Products); anti–protein disulfide isomerase (PDI; StressGen Biotechnologies); and anti–dynein intermediate chain (Chemicon). The anti-KIFC3 polyclonal antibody was raised in rabbits (Noda et al., 2001).

Scoring of Golgi apparatus distribution

To quantify the scattering degree of BODIPY-ceramide–positive pixels, we first classified into either object group or background by setting the threshold as 100. Then the coordinate of the object (*Xi*, *Yi*) was determined by NIH image Macros in each cell, followed by calculating the average center of all the objects for each cell. Finally, we transformed the total distances between each object and the center into the scattering degree. We compared the scattering degree in 100 each of wild-type and *kifC3*$^{-/-}$ cells. For dynamitin overexpression, adrenocortical cells were infected with adenovirus expressing dynamitin fusion proteins at 37°C for different durations of time and were stained with BODIPY-ceramide. The phenotype of the Golgi apparatus was assessed and the fluorescence intensity of dynamitin–CFP was recorded simultaneously. Cells with one or two juxtanuclear Golgi structures were scored as compact and others as dispersed.

Time-lapse imaging and FRAP experiments

A mixture of BODIPY-ceramide and BSA was prepared in MEM with 10 mM Hepes and processed as previously described (Pagano and Martin, 1994). Cells were observed using an Axiovert 100 (ZEISS) equipped with an MRC 1024 confocal laser scanning microscope (Bio-Rad Laboratories), as described previously (Nakata et al., 1998). The time-lapse sequence was recorded using Macros program (Bio-Rad Laboratories). FRAP was performed using MRC 1000 CLSM (Bio-Rad Laboratories) with the 488-nm line of the Kr/Ar laser. A small rectangular area set on the monitor was photobleached at full laser power (100% power, 100% transmission), and subsequent data collection was performed under 10% of laser power (Nakata et al., 1998).

Image analysis of Golgi apparatus movement

Time-lapse images of Golgi fragments labeled with BODIPY-ceramide were analyzed using an NIH image program. A mark was placed at the center of an individual fragment to record its pathway using Macros program. We followed the movement of 100 spots total for 2 h at 1-min intervals. The movements of each spot were scored as inward, outward, or a pause between each frame until the spot finally fused with the Golgi apparatus. The percentage of inwardly directed movement, outwardly directed movement, and pauses were calculated for each spot. The average percentage of 100 such independent spots was determined in 10 cells. The data in Table I were recorded from 20 to 70 min after BFA washout. Before 20 min, spots were difficult to distinguish. We followed the movement of individual fragments, and run lengths were measured until they stopped or changed the direction of movement (Nakata et al., 1998). Among the run lengths of a single fragment, the largest value was defined as the maximum run length. Approximately 100 spot traces were monitored in 10 cells of each group. Data are derived from three independent experiments.

Analysis of ER-to-Golgi transport

Adrenocortical cells were transfected with cDNA of VSVG tsO45–EGFP and incubated for 6 h at 39.5°C. Transport was initiated by incubating the cells at 30°C, and were recorded by CLSM (MRC-1024). Background intensities were subtracted from fluorescent intensities of both the Golgi apparatus and the entire cell area, which were plotted at different time points as described previously (Zaal et al., 1999). For the experiments using nocodazole, cells were incubated with 33 μM nocodazole for 2 h at 39.5°C. The transport was then observed during the next 30 min at 30°C.

Cell fractionation and immunoprecipitation

The Y1 cell line is derived from mouse adrenal cortex tissue (Riken Cell Bank), grown in the same condition as primary adrenocortical cells. The membrane-bound fraction was isolated by centrifugation at 100,000 *g* for 60 min and the supernatant was precipitated by TCA. Differential detergent extraction was performed as described previously (Hollenbeck, 1989). In brief, confluent Y1 cells were covered with buffer containing 0.1 M Pipes (pH 7.2), 5 mM $MgSO_4$, 10 μM EGTA, 2 mM DTT, protease inhibitors, 4% polyethylene glycol, 10 μM taxol, and 0.02% saponin for 10 min at 37°C. The buffer was removed and replaced with the same buffer containing 1% Triton X-100 instead of saponin. After 3 min, the buffer was recovered. CyDy and KIFC3 were recovered from the saponin- or Triton X-100–solubilized fraction by immunoprecipitation with anti-KIFC3 and anti–dynein intermediate chain antibodies (Noda et al., 2001). CyDy and KIFC3 in each fraction were quantified after Western blotting.

Online supplemental material

The time-lapse experiments shown in Fig. 5 (E and F), Fig. 6 (A and B), and Fig. 9 (A–H) are also viewable as Quick-Time videos (available at http://www.jcb.org/cgi/content/full/jcb.200202058/DC1). Videos 1 and 2 show the recovery phase of Golgi membranes after nocodazole washout. Videos 3 and 4 show the recovery process after BFA washout. Video 5 shows the VSVG–GFP transport from the ER to the Golgi apparatus in wild-type and *kifC3*$^{-/-}$ cells. Video 6 shows the VSVG–GFP dynamics in the presence of nocodazole in both cells.

We are grateful to Dr. H.P. Hauri for providing antibodies. We thank Drs. Y. Kanai, Y. Takei, A. Harada, Y. Okada, C. Zhao, J.L. Teng, and N. Homma (University of Tokyo) for assistance in transgenic technology and H. Fukuda, H. Sato, Y. Sugaya, and N. Onouchi for their technical and secretarial assistance.

This work was supported by a special grant-in-aid for the Center of Excellence from the Japanese Ministry of Education, Science, Sports, Culture, and Technology (N. Hirokawa), and Suzuki and Uehara fellowships (Y. Xu).

Submitted: 13 February 2002
Revised: 17 June 2002
Accepted: 17 June 2002

References

Allan, V.J., and T.A. Schroer. 1999. Membrane motors. *Curr. Opin. Cell Biol.* 11: 476–482.

Burkhardt, J.K., C.J. Echeverri, T. Nilsson, and R.B. Vallee. 1997. Overexpression of the dynamitin (p50) subunit of the dynactin complex disrupts dynein-dependent maintenance of membrane organelle distribution. *J. Cell Biol.* 139:469–484.

Cole, N.B., N. Sciaky, A. Marotta, J. Song, and J. Lippincott-Schwartz. 1996. Golgi dispersal during microtubule disruption: regeneration of Golgi stacks

at peripheral endoplasmic reticulum exit sites. *Mol. Biol. Cell.* 7:631–650.

De Camilli, P., S.D. Emr, P.S. McPherson, and P. Novick. 1996. Phosphoinositides as regulators in membrane traffic. *Science.* 271:1533–1539.

Echard, A., F. Jollivet, O. Martinez, J.J. Lacapere, A. Rousselet, I. Janoueix-Lerosey, and B. Goud. 1998. Interaction of a Golgi-associated kinesin-like protein with Rab6. *Science.* 279:580–585.

Hailstones, D., L.S. Sleer, R.G. Parton, and K.K. Stanley. 1998. Regulation of caveolin and caveolae by cholesterol in MDCK cells. *J. Lipid. Res.* 39:369–379.

Hanada, K., M. Nishijima, Y. Akamatsu, and R.E. Pagano. 1995. Both sphingolipids and cholesterol participate in the detergent insolubility of alkaline phosphatase, a glycosylphosphalidylinositol-anchored protein, in mammalian membranes. *J. Biol. Chem.* 270:6254–6260.

Hanlon, D.W., Z. Yang, and L.S. Goldstein. 1997. Characterization of KIFC2, a neuronal kinesin superfamily member in mouse. *Neuron.* 18:439–451.

Harada, A., K. Oguchi, S. Okabe, I. Kuno, S. Terada, T. Ohnishi, R. Sato-Yoshitake, Y. Takei, T. Noda, and N. Hirokawa. 1994. Altered microtubule organization in small-calibre axons of mice lacking tau protein. *Nature.* 369: 488–491.

Harada, A., Y. Takei, Y. Kanai, Y. Tanaka, S. Nonaka, and N. Hirokawa. 1998. Golgi vesiculation and lysosome dispersion in cells lacking cytoplasmic dynein. *J. Cell Biol.* 141:51–59.

Hirokawa, N. 1998. Kinesin and dynein superfamily proteins and the mechanism of organelle transport. *Science.* 279:519–526.

Ho, W.C., V.J. Allan, G. van Meer, E.G. Berger, and T.E. Kreis. 1989. Reclustering of scattered Golgi elements occurs along microtubules. *Eur. J. Cell Biol.* 48:250–263.

Hollenbeck, P.J. 1989. The distribution, abundance and subcellular localization of kinesin. *J. Cell Biol.* 108:2335–2342.

Holleran, E.A., L.A. Ligon, M. Tokito, M.C. Stankewich, I.S. Morrow, and E.I. Holzbaur. 2001. βIII spectrin binds to the Arp1 subunit of dynactin. *J. Biol. Chem.* 276:36598–36605.

Hurley, J.H., and T. Meyer. 2001. Subcellular targeting by membrane lipids. *Curr. Opin. Cell Biol.* 13:146–152.

Infante, C., F. Ramos-Morales, C. Fedriani, M. Bornens, and R.M. Rios. 1999. GMAP-210, a cis-Golgi network-associated protein, is a minus end microtubule-binding protein. *J. Cell Biol.* 145:83–98.

Keller, P., and K. Simons. 1998. Cholesterol is required for surface transport of influenza virus hemagglutinin. *J. Cell Biol.* 140:1357–1367.

Kilsdonk, E.P., P.G. Yancey, G.W. Stoudt, F.W. Bangerter, W.J. Johnson, M.C. Phillips, and G.H. Rothblat. 1995. Cellular cholesterol efflux mediated by cyclodextrins. *J. Biol. Chem.* 270:17250–17256.

Kobayashi, T., M.H. Beuchat, M. Lindsay, S. Frias, R.D. Palmiter, H. Sakuraba, R.G. Parton, and J. Gruenberg. 1999. Late endosomal membranes rich in lysobisphosphatidic acid regulate cholesterol transport. *Nat. Cell Biol.* 1:113–118.

Lane, J.D., J. Lucocq, J. Pryde, F.A. Barr, P.G. Woodman, V.J. Allan, and M. Lowe. 2002. Caspase-mediated cleavage of the stacking protein GRASP65 is required for Golgi fragmentation during apoptosis. *J. Cell Biol.* 156:495–509.

Lin, S.X., K.L. Ferro, and C.A. Collins. 1994. Cytoplasmic dynein undergoes intracellular redistribution concomitant with phosphorylation of the heavy chain in response to serum starvation and okadaic acid. *J. Cell Biol.* 127: 1009–1019.

Lippincott-Schwartz, J., L.C. Yuan, J.S. Bonifacino, and R.D. Klausner. 1989. Rapid redistribution of Golgi proteins into the ER in cells treated with brefeldin A: evidence for membrane cycling from Golgi to ER. *Cell.* 56:801–813.

Lippincott-Schwartz, J., N. Cole, and J. Presley. 1998. Unraveling Golgi membrane traffic with green fluorescent protein chimeras. *Trends Cell Biol.* 8:16–20.

Miller, R.G. 1984. The use and abuse of filipin to localize cholesterol in membranes. *Cell. Biol. Int. Rep.* 8:519–535.

Nakata, T., S. Terada, and N. Hirokawa. 1998. Visualization of the dynamics of synaptic vesicle and plasma membrane proteins in living axons. *J. Cell Biol.* 140:659–674.

Noda, Y., Y. Okada, N. Saito, M. Setou, Y. Xu, Z. Zhang, and N. Hirokawa. 2001. KIFC3, a microtubule minus end–directed motor for the apical transport of annexin XIIIb-associated triton-insoluble membranes. *J. Cell Biol.* 155:77–88.

Pagano, R.E., and O.C. Martin. 1994. Use of fluorescent analogs of cermide to study the Golgi apparatus of animal cells. *In* Cell Biology. A Laboratory Handbook. J.E. Celis, editor. Academic Press Inc. San Diego, CA. 387–394.

Presley, J.F., N.B. Cole, T.A. Schroer, K. Hirschberg, K.J. Zaal, and J. Lippincott-Schwartz. 1997. ER-to-Golgi transport visualized in living cells. *Nature.* 389:81–85.

Ramachandran, J., and A.T. Suyama. 1975. Inhibition of replication of normal adrenocortical cells in culture by adrenocorticotropin. *Proc. Natl. Acad. Sci. USA.* 72:113–117.

Rothman, J.E., and F.T. Wieland. 1996. Protein sorting by transport vesicles. *Science.* 272:227–234.

Saito, N., Y. Okada, Y. Noda, Y. Kinoshita, S. Kondo, and N. Hirokawa. 1997. KIFC2 is a novel neuron-specific c-terminal type kinesin superfamily motor for dendritic transport of multivesicular body-like organelles. *Neuron.* 18: 425–438.

Schroer, T.A. 2000. Motors, clutches and brakes for membrane transport: a commemorative review in honor of Thomas Kreis. *Traffic.* 1:3–10.

Schweizer, A., J.A.M. Fransen, T. Bachi, L. Ginsel, and H.P. Hauri. 1988. Identification, by a monoclonal antibody, of a 53-kD protein associated with a tubulo-vesicular compartment at the cis-side of the Golgi apparatus. *J. Cell Biol.* 107:1643–1653.

Stearns, T. 1997. Motoring to the finish: kinesin and dynein work together to orient the yeast mitotic spindle. *J. Cell Biol.* 138:957–960.

Takei, Y., I. Teng, A. Harada, and N. Hirokawa. 2000. Defects in axonal elongation and neuronal migration in mice with disrupted tau and map 1b genes. *J. Cell Biol.* 150:989–1000.

Teng, I., Y. Takei, A. Harada, T. Nakata, I. Chen, and N. Hirokawa. 2001. Synergistic effects of MAP2 and MAP1B knockout in neuronal migration, dendritic outgrowth, and microtubule organization. *J. Cell Biol.* 155:65–76.

Vaisberg, E.A., B.M. Grisson, and J.R. McIntosh. 1996. Mammalian cells express three distinct dynein heavy chains that are localized to different cytoplasmic organelles. *J. Cell Biol.* 133:831–842.

Valderrama, F., J.M. Duran, T. Babia, H. Barth, J. Renau-Piqueras, and G. Egea. 2001. Actin microfilaments facilitate the minus-end directed transport from the Golgi complex to the endoplasmic reticulum in mammalian cells. *Traffic.* 2:717–726.

Ward, T.H., R.S. Polishchuk, S. Caplan, K. Hirschberg, and J. Lippincott-Schwartz. 2001. Maintenance of Golgi structure and function depends on the integrity of ER export. *J. Cell Biol.* 155:557–570.

Yang, Z., C. Xia, E.A. Roberts, K. Bush, S.K. Nigam, and L.S.B. Goldstein. 2001. Molecular cloning and functional analysis of mouse c-terminal kinesin motor kifC3. *Mol. Cell. Biol.* 21:765–770.

Zaal, K.J., C.L. Smith, R.S. Polishchuk, N. Altan, N.B. Cole, J. Ellenberg, K. Hirschberg, J. Presley, T.H. Roberts, E. Siggia, et al. 1999. Golgi membranes are absorbed into and reemerge from the ER during mitosis. *Cell.* 99: 589–601.